

Development of electromagnetic pellet injector for disruption mitigation of tokamak plasma

Feng Li(李峰), Zhong-Yong Chen(陈忠勇), Sheng-Guo Xia(夏胜国), Wei Yan(严伟), Wei-Kang Zhang(张维康), Jun-Hui Tang(唐俊辉), You Li(李由), Yu Zhong(钟昱), Jian-Gang Fang(方建港), Fan-Xi Liu(刘凡溪),Gui-Nan Zou(邹癸南), Yin-Long Yu(喻寅龙), Zi-Sen Nie(聂子森), Zhong-He Jiang(江中和),Neng-Chao Wang(王能超), Yong-Hua Ding(丁永华), Yuan Pan(潘垣), and the J-TEXT team

Citation: Chin. Phys. B, 2023, 32 (**7**): 075205. DOI: 10.1088/1674-1056/acc7fb
Journal homepage: http://cpb.iphy.ac.cn; http://iopscience.iop.org/cpb

What follows is a list of articles you may be interested in

Disruption prediction based on fusion feature extractor on J-TEXT

Wei Zheng(郑玮), Fengming Xue(薛凤鸣), Zhongyong Chen(陈忠勇), Chengshuo Shen(沈呈硕), Xinkun Ai(艾鑫坤), Yu Zhong(钟昱), Nengchao Wang(王能超), Ming Zhang(张明),Yonghua Ding(丁永华), Zhipeng Chen(陈志鹏), Zhoujun Yang(杨州军), and Yuan Pan(潘垣)

Chin. Phys. B, 2023, 32 (**7**): 075203. DOI: 10.1088/1674-1056/acc7fc

Gyrokinetic simulation of low-*n* Alfvénic modes in tokamak HL-2A plasmas

Wen-Hao Lin(林文浩), Ji-Quan Li(李继全), J Garcia, and S Mazzi

Chin. Phys. B, 2023, 32 (**2**): 025202. DOI: 10.1088/1674-1056/ac6b23

Linear analysis of plasma pressure-driven mode in reversed shear cylindrical tokamak plasmas

Ding-Zong Zhang(张定宗), Xu-Ming Feng(冯旭铭), Jun Ma(马骏), Wen-Feng Guo(郭文峰), Yan-Qing Huang(黄艳清), and Hong-Bo Liu(刘洪波)

Chin. Phys. B, 2023, 32 (**1**): 015201. DOI: 10.1088/1674-1056/ac70b4

Parametric decay instabilities of lower hybrid waves on CFETR

Taotao Zhou(周涛涛), Nong Xiang(项农), Chunyun Gan(甘春芸), Guozhang Jia(贾国章), and Jiale Chen(陈佳乐)

Chin. Phys. B, 2022, 31 (**9**): 095201. DOI: 10.1088/1674-1056/ac67c2

Modeling of beam ions loss and slowing down with Coulomb collisions in EAST

Yifeng Zheng(郑艺峰), Jianyuan Xiao(肖建元), Baolong Hao(郝保龙), Liqing Xu(徐立清), Yanpeng Wang(王彦鹏), Jiangshan Zheng(郑江山), and Ge Zhuang(庄革)

Chin. Phys. B, 2022, 31 (**7**): 075201. DOI: 10.1088/1674-1056/ac5883

SPECIAL TOPIC — Plasma disruption

Development of electromagnetic pellet injector for disruption mitigation of tokamak plasma

Feng Li(李峰)[1], Zhong-Yong Chen(陈忠勇)[1,†], Sheng-Guo Xia(夏胜国)[2], Wei Yan(严伟)[1], Wei-Kang Zhang(张维康)[1], Jun-Hui Tang(唐俊辉)[2], You Li(李由)[1], Yu Zhong(钟昱)[1], Jian-Gang Fang(方建港)[1], Fan-Xi Liu(刘凡溪)[1], Gui-Nan Zou(邹癸南)[1], Yin-Long Yu(喻寅龙)[1], Zi-Sen Nie(聂子森)[1], Zhong-He Jiang(江中和)[1], Neng-Chao Wang(王能超)[1], Yong-Hua Ding(丁永华)[1], Yuan Pan(潘垣)[1], and the J-TEXT team[1,‡]

[1] *International Joint Research Laboratory of Magnetic Confinement Fusion and Plasma Physics, State Key Laboratory of Advanced Electromagnetic Engineering and Technology, School of Electrical and Electronic Engineering, Huazhong University of Science and Technology, Wuhan* 430074, *China*

[2] *Key Laboratory of Pulsed Power Technology Ministry of Education Huazhong University of Science and Technology, School of Electrical and Electronic Engineering, Huazhong University of Science and Technology, Wuhan* 430074, *China*

(Received 21 December 2022; revised manuscript received 16 March 2023; accepted manuscript online 28 March 2023)

Disruption remains to be a serious threat to large tokamaks like the International Thermonuclear Experimental Reactor (ITER). The injection speed of disruption mitigation systems (DMS) driven by high pressure gas is limited by the sound speed of the propellant gas. When extrapolating to ITER-like tokamaks, long overall reaction duration and shallow penetration depth due to low injection speed make it stricter for plasma control system to predict the impending disruptions. Some disruptions with a short warning time may be unavoidable. Thus, a fast time response and high injection speed DMS is essential for large scale devices. The electromagnetic pellet-injection (EMPI) system is a novel massive material injection system aiming to provide rapid and effective disruption mitigation. Based on the railgun concept, EMPI can accelerate the payload to over 1000 m/s and shorten the overall reaction time to a few milliseconds. To verify the injection ability and stability of the EMPI, the prototype injector EMPI-1 has been designed and assembled. The preliminary test has been carried out using a 5.9 g armature to propel a dummy pellet and the results suggest that the EMPI configuration has a great potential to be the DMS of the large scale fusion devices.

Keywords: tokamak, disruption mitigation system, electromagnetic pellet-injection (EMPI)

PACS: 52.55.Fa **DOI:** 10.1088/1674-1056/acc7fb

1. Introduction

Although multiple methods have been taken to control the burning plasma, disruption still remains inevitable during the operation of tokamaks. When disruption occurs on large scale devices, unbearable heat load would deposit on plasma facing components (PFCs) during thermal quench (TQ). The following current quench (CQ) could induce great electromagnetic (EM) force on metal components. Moreover, in the case of the International Thermonuclear Experimental Reactor (ITER) up to 10 MA of runaway electron current generated during the current decay would deposit on the first wall (FW) and melt the FW material. Thus, disruptions without any mitigation would cause great damage and shorten the lifetime of the fusion reactors, making it an urgent issue for fusion reactors to mitigate disruptions.[1,2]

The common method for disruption mitigation is to trigger rapid shutdown by massive material injection.[3] Experiments and simulations both suggest that the disruption effects can be mitigated if needed quantity of impurity particles can penetrate into the plasma core and be assimilated. Massive gas injection (MGI) uses electromagnetic valve to release impurity gas into the plasma to mitigate the heat load and reduce the EM force. But the injected gas could not penetrate deeply into the plasma on large scale device with high performance operation and the cold front would pre-trigger the TQ, leading to poor impurity assimilation rate. Instead of gas injection, shattered pellet injection (SPI) freezes the impurity gas into cryogenic pellet in the gun barrel and pneumatically accelerates the pellet. At the end of the barrel, the pellet would be shattered by the bent tube and injected into the plasma. Compared to MGI, shattered pellet can penetrate more deeply and sharply. Most of the impurity would be assimilated and weaken the conducted heat fluxes.[4–7] However, DMS for high-performance reactors should be capable of not only delivering impurities into the plasma, but also reacting in time and finishing the injection before disruption occurs.[8] DMS is triggered by disruption detection system and the triggering lead time should cover the overall reaction time of DMS. With the extension of the triggering lead time, the reliability of the disruption detection system drops sharply.[9] Both MGI and SPI are gas propellent systems and the injection speed is limited by the sound speed of the propellent gas. Meanwhile the pellet flight tube on ITER-like fusion reactors is much longer than any current

†Corresponding author. E-mail: zychen@mail.hust.edu.cn

‡See the author list of " Wang N *et al.* 2022 *Nucl. Fusion* **62** 042016"

© 2023 Chinese Physical Society and IOP Publishing Ltd

devices, making the overall reaction time longer than 30 ms.[2] In this case, the success rate of the disruption detection system is relatively low. What's more, in the case of ITER, the distance from the plasma edge to the magnetic axis is 2 m, and the estimated TQ duration is 2 ms–3 ms, meaning that the pellet velocity should be at least 1 km/s, which is far beyond the SPI velocity. Thus, a fast acting, high velocity and reliable injector is quite needed for the ITER DMS.

In 1983, railguns were nominated by Hawk as fusion fuel pellet injector[10] for their potential advantage in high injection speed of over 10 km/s. Comparing to pneumatic injector, a railgun injector could accelerate the payload to a guaranteed high speed without putting much pressure on the gas system. Moreover, the pellet acceleration duration for a railgun injector could be less than 4 ms comparing to over 10 ms via pneumatic injector.[11] Thus, if a railgun system is used in DMS instead of pneumatic injector, the injection speed and the overall response time could be greatly improved. Similar fueling injector like compact torus injection system has also been applied in fusion devices,[12] showing that an electromagnetic device is feasible in the application of fusion devices. R. Raman had also given a more detailed discussion towards the advantage of a railgun system.[13–15] With the promised advantages mentioned above and less impurities produced, a railgun injector is quite suitable for DMS.

To achieve higher injection speed and be capable of meeting the short warning time for DMS, electromagnetic particle injector (EPI) concept is carried out. Based on the electromagnetic railgun theory, EPI could propellent a 12 g pellet to 1 km–2 km in 2 ms in theory. Significant progress has been made further the concept to prototype test and successfully separating the payload ball from sabot at the speed of 200 m/s.[13–15] However, there are still a set of difficulties before a railgun system could be tested on a tokamak. A railgun injector is mainly composed of power storage capacitors, bus bars, rails and armature. Acting as the energy converter, armature needs to carry the payload (impurity pellet) to over 1 km/s and release the payload before being collected. So, how to safely block and collect the armature without any possible damage needs more exploration. How to reliably separate the payload from the armature at a high velocity and ensure a stable trajectory should be considered. During the injection, up to 100 kA current would flow through the rails and armature, generating a quantity of unwanted impurities. Therefore, the elimination of the unwanted impurities should also be considered.

To solve the difficulties mentioned above and explore a high-speed massive material injection system for ITER-like fusion reactors, an electromagnetic pellet-injection system (EMPI) configuration is proposed. The novel configuration takes the advantage of reverse electromagnetic force by introducing deceleration gun barrel into typical railgun system. The configuration enables the in-bore release of the payload and controllable armature deceleration. To verify the effects of the configuration, an EMPI prototype platform has been established and preliminary tests have also been carried out including armature acceleration tests, armature deceleration tests and armature and payload separation tests. The details will be described below.

2. EMPI configuration for massive material injection

Basically, EMPI configuration is formed by reverse concatenating two railguns. Figure 1 shows the schematic diagram of EMPI configuration. Apart from a conventional railgun system, another pulse power supply is applied at the muzzle of the railgun to form a deceleration railgun barrel. The power supply for deceleration would be triggered right after the acceleration process and generate a decelerating $\boldsymbol{J} \times \boldsymbol{B}$ force on the armature reverse to the flight direction. The decelerating force then drags the armature to a relatively low velocity before flying out of the barrel. Equipped with the deceleration railgun barrel, the deceleration process could be controllable by adjusting the current flow thus taking control of the armature muzzle speed. Another advantage lies in the separation between the armature and the payload. As the electromagnetic force acts on the armature, the payload is only fixed by the friction force which can be neglected compared to the electromagnetic force. Hence the payload would divorce from the armature and rely on its own inertia without dropping much velocity. As the separation would take place in the barrel and the armature trajectory is restricted by the rails, the payload trajectory would also be restricted during the separation. With the restriction mentioned above, the payload would be released and fly through the tube without much deviation.

To be deployed near the tokamak, the launching and breaking process will be impacted by the magnetic field around the tokamak. The strong stray field would interact with the armature current and generate an additional force on the armature. According to the direction of the additional force, the impact can be divided into three cases. The first case is that the additional force is opposite to the launching or breaking force, which leads to a reduction in launch efficiency and shortens the lifetime of the rail electrodes. In the second case, the additional force is biased towards one side of the rails, leading to an asymmetrical armature-rail contact. The contact force on one side of the contact surface is offset by additional force, resulting in contact transition and destabilizing the launching and the breaking. The first two cases can be avoided by deploying the EMPI some distance away from the tokamak and adding an electromagnetic shielding. Correspondingly, the overall response time would slightly increase. The third case is that the

additional force is in the same direction with the launching or breaking force. By adjusting the direction of the rail current flow, the magnetic field between the rails can superimpose on the ambient magnetic fields. With the enhancement of the magnetic fields, the injection efficiency can raise greatly, and the needed current flow could also be reduced. In addition, the EMPI can be deployed near the vacuum vessel thus shortening the overall reaction time. The deployment concept of a railgun system was also discussed in the Raman's work.[15]

To verify the EMPI configuration, numerical calculations are performed based on

$$\boldsymbol{F} = \frac{1}{2}\boldsymbol{L}'I^2, \tag{1}$$

where $\boldsymbol{F}$ is the electromagnetic force acting on the armature, $\boldsymbol{L}'$ is the inductance gradient of the rails, and I is the current flow in the circuit.

With given current waveforms (typical waveforms generated by the three 27 mF capacitors with a charging voltage of 1000 V–7500 V when connecting with a similar railgun circuit load), velocities and displacements of the armature and the payload are calculated. In the calculation, accelerating rail electrodes and decelerating rail electrodes are isolated from each other and each of the lengths is 1.5 m. The inductance gradient of the rails is 0.4 μH/m according to electromagnetic field simulation of single-rail prototype model. The mass of the armature is 5.9 g and the mass of the payload is 100 mg in the case of carbon pellet injection for J-TEXT tokamak. The calculation results are shown in Fig. 2. According to Fig. 2(a), a velocity of over 1000 m/s can be reached accelerated by the current with a peak value of 194 kA in merely 2.4 ms. Decelerated by a same current with a proper time delay, the muzzle velocity can drop to 300 m/s. A lower muzzle velocity could also be achieved by shortening the time delay or increasing the charging voltage of the deceleration power source. The displacement of the payload in 10 ms is about 10 m. With a flight tube length of 6.3 m for ITER,[2] the EMPI configuration can meet the overall reaction time demand. To experimentally verify the configuration, a prototype has also been constructed and the test results are described in Section 3.

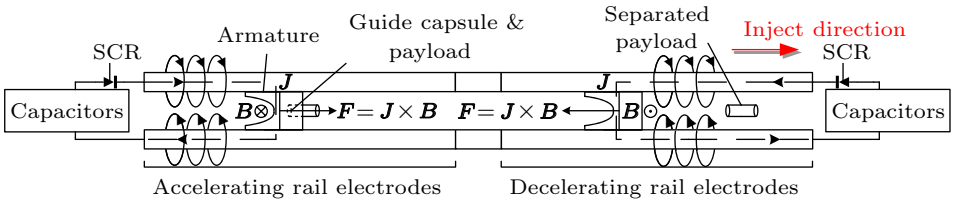


Fig. 1. EMPI configuration.

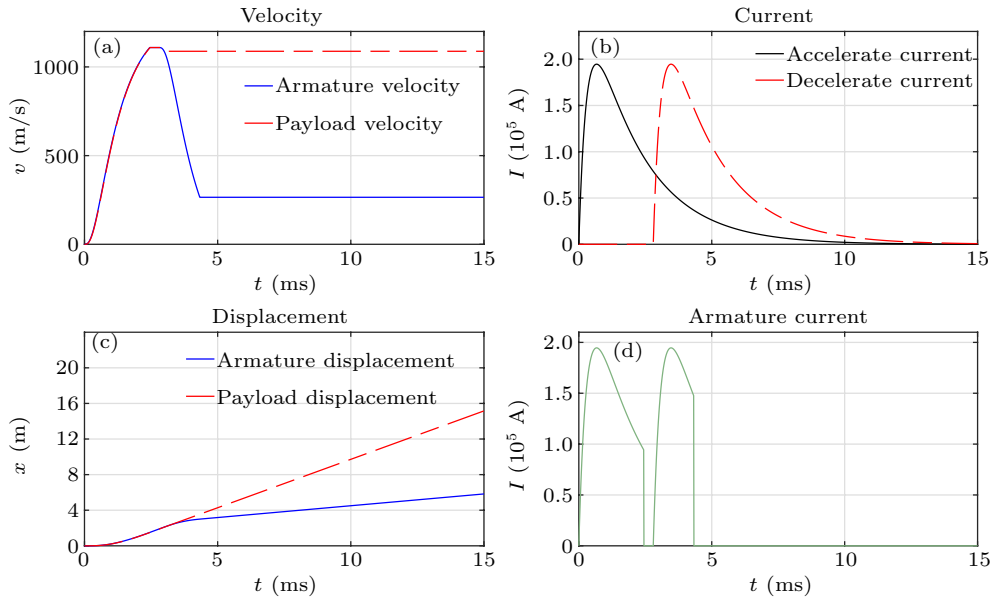


Fig. 2. Traces from calculation results: (a) calculated armature velocity (blue line) and pellet 8 velocity (red dash line), (b) acceleration rail current (black line) and deceleration rail current (red 9 dash line), (c) displacement of the armature (blue line) and the payload (red dash), (d) armature 10 current flow, all as a function of time.

3. Prototype of EMPI for J-TEXT

Motivated by the numerical analysis, a prototype injector of EMPI configuration is designed and constructed. Figure 3 illustrates the prototype of EMPI and Fig. 4 shows the EMPI prototype test platform. To realize the remote control and data acquisition of the launching process, an armature loading system and a data acquisition and trigger timing system

have been established. The armature loader is mounted at the end of the acceleration barrel. As the prototype is tested under the atmospheric environment, the loader is hydraulically powered, and a putter is installed in the head of the hydraulic press. When loading, the putter will be driven by the hydraulic press to thrust the armature through the preloading bore into the launching position. Figure 5 shows the C-type armature tested during the experiment. The head of the putter is specially designed to fit the throat of the armature. The preloading bore is a designed slope slightly lower than the slope angle of the armature tail. With the application of the putter head and the preloading bore, the armature would maintain a symmetrical posture while loading, and the asymmetrical launch can be greatly avoided compared to manual load.

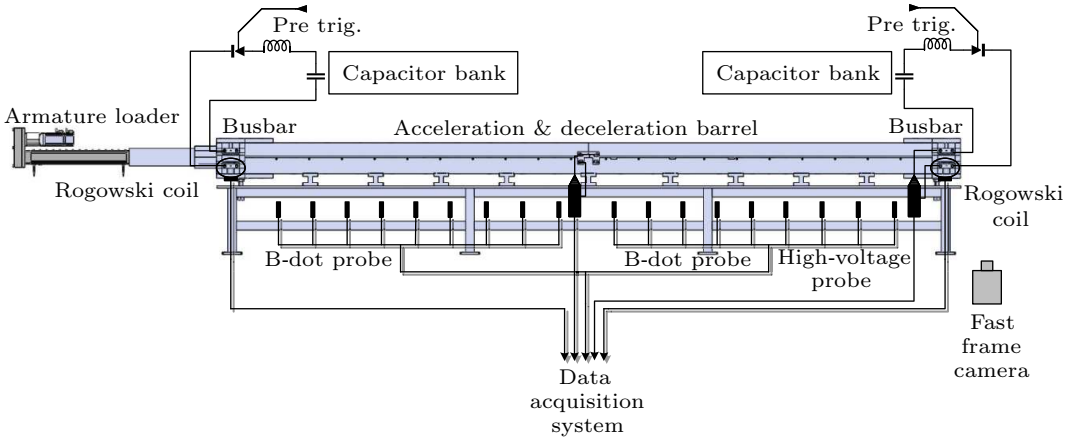


Fig. 3. Schematic of the prototype EMPI, including the auxiliary component and diagnostics.



Fig. 4. EMPI prototype test platform.

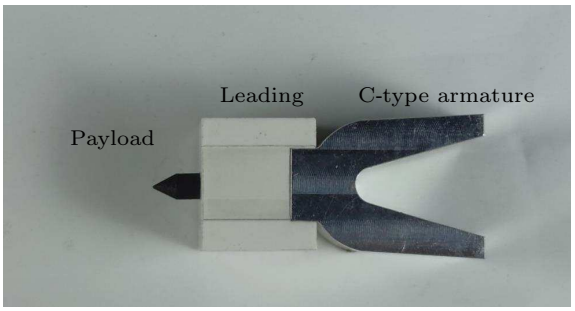


Fig. 5. C-type armature with payload and leading.

The prototype is a single-rail railgun and the main parameters of the EMPI prototype test platform are shown in Table 1. The caliber of the prototype is 14 mm × 12 mm. Busbar at each end of the gun barrel is connected to three 27 mF, 7.5 kV capacitors through coaxial-cables. All the capacitors are switched by silicon controlled rectifier (SCR) and a laser trigger system is applied to take control of the trigger timing. Each rail is composed of an inner rail and an outer rail as shown in Fig. 6. The outer rail is compressed with the bus bar and the inner rail is directly contact with the armature. By dividing each rail into two layers, only the inner rail would be ablated while the outer rail would be intact. Eighteen B-dot probes are installed at one side of the barrel to obtain the armature displacement. B-dot probe is a small conductive loop, which produces an output voltage proportional to the time rate of change of the magnetic flux linking the loop. The loop is placed between the rails and parallels to the current flow of the armature and the magnetic flux linking the loop is only generated by the armature current. In this configuration, the zero-crossing point is usually taken to be the time when the armature is right under the position of the probe. A fast frame camera is also placed at the muzzle to record the motion of the payload and the armature.

Table 1. C-type armature with payload and leading.

Parameter	
Rail material	copper
Rail length (m)	3
Caliber (mm)	14 × 12
Accelerating bank capacitance (mF)	27 × 3
Decelerating bank capacitance (mF)	27 × 3
Accelerating bank voltage (kV)	0.2–7.5
Decelerating bank voltage (kV)	0.2–7.5
Armature mass (g)	5.9
Armature material	aluminum
Payload mass (mg)	100

During the first stage of the bench test, the rails for ac-

celeration and deceleration are isolated by a pair of 200 mm long blocks. Each rail is 1.5 m in length with an electrode gap separation of 14 mm. However, severe muzzle arc is induced as the residual energy is still considerable when the armature is flying out of the acceleration barrel. The induced muzzle arc can influence the launching stability and aggravate the ablation of the armature and rails. The ablated armature could not keep in well contact with rails, leading to transition inside the bore. A great deal of ablated material is generated due to transition. Part of the ablated material would deposit onto the surface of the rail, causing an uneven contact surface for the subsequent launching. Other ablated material would transport with payload and armature through the bore and shunt the armature current, causing a failed deceleration. Finally, the ablated material would jet out of the muzzle and turn into undesirable impurity for tokamak application.

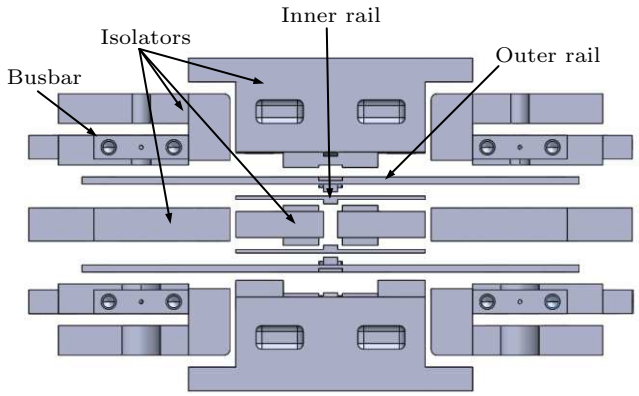


Fig. 6. The exploded view of prototype EMPI.

Thus, isolation blocks are removed, and two pairs of rails are bonded together into a long pair of rails called sharing rail. An arc suppression system is also designed and mounted onto the muzzle to consume the residual energy. By using sharing rails, acceleration muzzle is eliminated and there is no critical separation between acceleration rail electrodes and deceleration electrodes. The current path for acceleration still remains during the deceleration process until the armature flying off the muzzle, then the current would flow through the arc suppression system and the residual energy would be consumed by arc suppression resistance.

Because of the remaining acceleration circuit during the deceleration stage, the deceleration of the armature is also influenced by the acceleration current flow. Figure 7 illustrates two connection modes for deceleration capacitor bank when sharing rails are applied. $\boldsymbol{J}_{\rm acc}$, $\boldsymbol{J}_{\rm dec}$, and $\boldsymbol{J}_{\rm arm}$ indicate the acceleration current, deceleration current and the current flow through the armature, respectively. $\boldsymbol{B}_{\rm acc}$ and $\boldsymbol{B}_{\rm dec}$ indicate the magnetic field generated by the rail current.

Figure 7(a) illustrates a current enhanced connection mode. The same polarity terminals of both acceleration capacitors and deceleration capacitors are connected to the same rail. As shown in the Fig. 7(a), the armature current $\boldsymbol{J}_{\rm arm} = \boldsymbol{J}_{\rm acc} + \boldsymbol{J}_{\rm dec}$ indicates that the armature current is enhanced by the acceleration current. However, $\boldsymbol{J}_{\rm acc}$ and $\boldsymbol{J}_{\rm dec}$ flowing in the rails are contrary to each other, thus the induced $\boldsymbol{B}_{\rm dec}$ is weakened by $\boldsymbol{B}_{\rm acc}$. Figure 7(b) illustrates a magnetic field enhanced connection mode. Two opposite polarity terminals are connected to each end of the rail. The magnetic fields induced by the rail current $\boldsymbol{J}_{\rm acc}$ and $\boldsymbol{J}_{\rm dec}$ enhance each other whereas the armature current $\boldsymbol{J}_{\rm arm} = \boldsymbol{J}_{\rm dec} - \boldsymbol{J}_{\rm acc}$ is weakened. Both connection modes have been experimentally tested and will be discussed in Section 4.

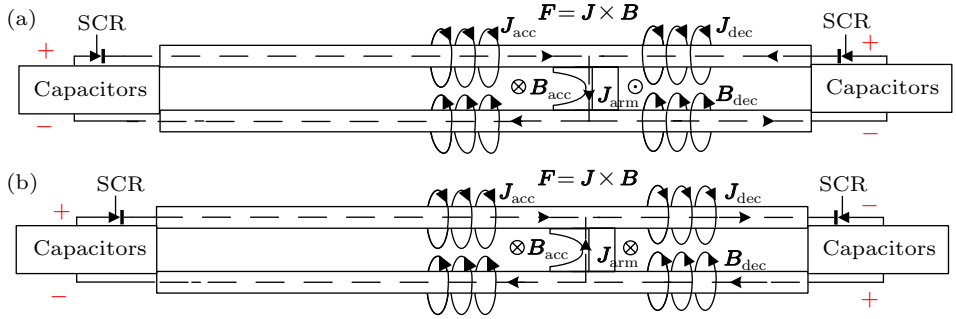


Fig. 7. (a) Illustrates the armature current enhanced circuit for sharing rails after deceleration capacitors are triggered. (b) Illustrates the magnetic field enhanced circuit for sharing rails after deceleration capacitors are triggered.

4. Preliminary results of EMPI prototype test

In order to test the launching performance, to verify the usability of the EMPI configuration in payload releasing and armature deceleration, a series of platform tests have been carried out including armature acceleration, armature deceleration and armature and payload separation. A typical test result acquired by the diagnostic system during armature acceleration tests is shown in Fig. 8 including (a) accelerating current waveform measured by Rogowski coil, (b) muzzle voltage measured by voltage divider, (c) armature position detected by B-dot probes and (d) muzzle velocity calculated from the position data. Basic launching parameters together with the contact condition can be obtained via the diagnostic system. Based on the data detected by B-dot probes, muzzle velocities are calculated and summarized in Fig. 9, abscissa axis represents the peak value of the acceleration current. A wide range

of muzzle velocity from 572 m/s to over 1200 m/s is obtained by adjusting the charged voltage of the capacitor bank. The results indicate that the muzzle velocity is positively correlated with the peak value of the current. The fluctuation of the muzzle velocity is mainly induced by the flatness of the rail surface after a number of shots. As the peak value of the current is linear to the voltage value of the capacitor bank. The muzzle velocity could be controlled by adjusting the charged voltage of the capacitor bank if the flatness of the rail surface could be guaranteed.

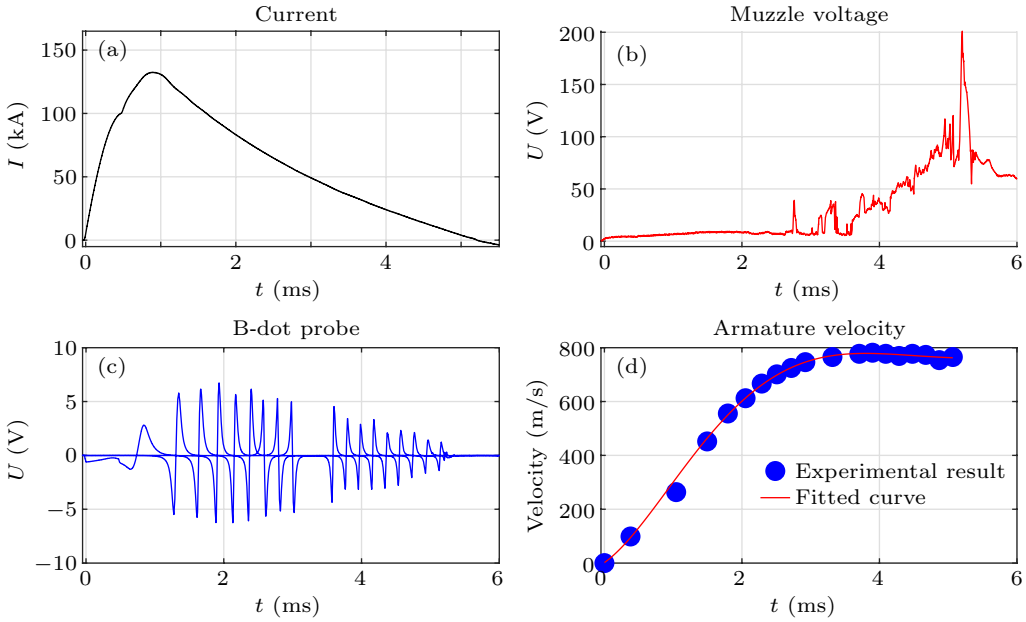


Fig. 8. Experimental data of a typical acceleration test: (a) measured rail currents, (b) measured muzzle voltage, (c) data acquired by B-dot probes, (d) armature velocity (blue dot) calculated by the data of B-dot probes and the fitted curve (red line) of the calculated velocity data.

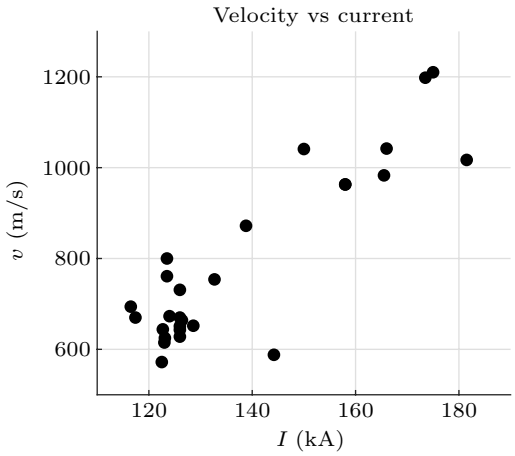


Fig. 9. Experimentally measured armature velocity versus the peak value of the rail current.

As an electromagnetic propulsion system, the fast time response ability is the one of the key advantages over other high-pressure gas propulsion systems. The summaries of acceleration duration are shown in Fig. 10(a). With the increase of muzzle velocity from 572 m/s to 1210 m/s, the acceleration duration decreases from 3.56 ms to 2.239 ms. Assuming that the flight tube of ITER and J-TEXT is 6.3 m and 3 m, respectively.[2] Based on the test results, the overall response time is calculated and summarized in Fig. 10(b). As for J-TEXT, an injection speed of over 572 m/s can lower the overall response time to 9 ms, approaching the response speed of J-TEXT MGI. In contrast, the overall response time of J-TEXT SPI is over 25 ms due to long tube away from the torus. Disruption mitigation experiments cooperating with disruption detection system could be possible if EMPI is applied on J-TEXT. As for the scale of ITER, with a maximum test speed of over 1200 m/s, the overall reaction time could be less than 10 ms. Meanwhile, the test results have shown a high consistency relationship between acceleration duration and muzzle velocity. Thus, by controlling the muzzle velocity, the overall response time can be guaranteed. It is necessary to note that the extrapolation from J-TEXT to ITER does not take the mass of the impurity pellet into account. As the required mass of the impurity is of the same order with the armature applied in the experiments. By increasing the injection current accordingly, the corresponding speed can also be achieved in the case of ITER.

The intention of the EMPI configuration is not only to achieve a high speed, fast response injection, but also to realize the reliable separation of the payload from the armature and then decelerating the high-speed armature to a relatively low speed before flying out of the muzzle and collecting. Thus, the armature deceleration tests are carried out and Fig. 11 shows a typical test results in comparison to the numerical calculation result. Figure 11(b) shows that the test result is roughly consistent with the calculated results during the acceleration process and the deceleration process under the applied current flow shown in Fig. 11(a). With a decelerating current of 112 kA

which is slightly lower than the accelerating current, the velocity of the armature drops from 731 m/s to around 100 m/s. Over 98% kinetic energy of the armature is consumed during the deceleration process. With a velocity of around 100 m/s, the armature can be easily landed without much threat to the chamber.

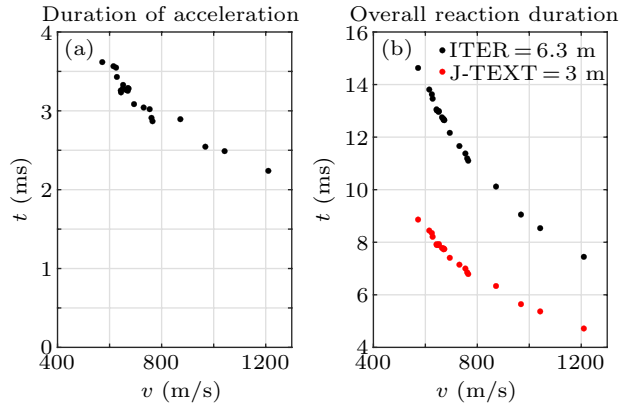


Fig. 10. (a) The acceleration duration of the corresponding velocity. (b) Overall reaction duration presuming the flight tube length is 6.3 m for ITER and 3 m for J-TEXT.

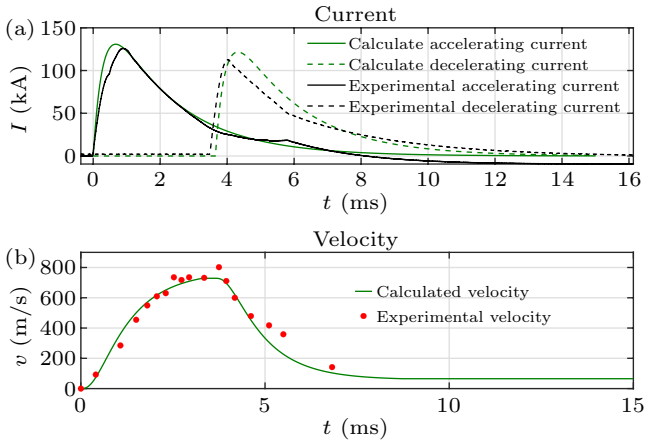


Fig. 11. (a) Applied current flows in the acceleration calculation (green line) and deceleration calculation (green dash line) are shown together with the experimental current flow of acceleration (black line) and deceleration (black dash line). (b) Comparison of calculated velocity (green line) and experimental velocity (red dot) under the current shown in panel (a).

It is necessary to note that the test result as shown in Fig. 11 was obtained with magnetic field enhanced connection mode rather than current enhanced connection mode. Figure 12 illustrates that the acceleration current decline rate drops after the trigger of deceleration capacitors in magnetic field enhanced connection mode. The decline rate of the deceleration current drops as well compared to the current enhanced connection mode. The prolonged rail current further decelerates the armature to a lower velocity. Repetitive tests are consistent with the result shown in Fig. 12. One of the possible explanations is that the linkage of the magnetic field increases the equivalent inductance of the circuit thus increasing the inductance gradient of the rail. In terms of the armature current changing, the current enhanced connection mode increases the armature current flow which would aggravate the ablation of the contact surface or even induce transition while the magnetic field enhanced connection mode reduces the armature current flow and results in an opposite effect. If an EMPI is installed near the device, the magnetic enhanced connection mode has the potential to take advantage of the biased magnetic field during both acceleration and deceleration processes. Thus, the magnetic enhanced mode seems to be more suitable for EMPI.

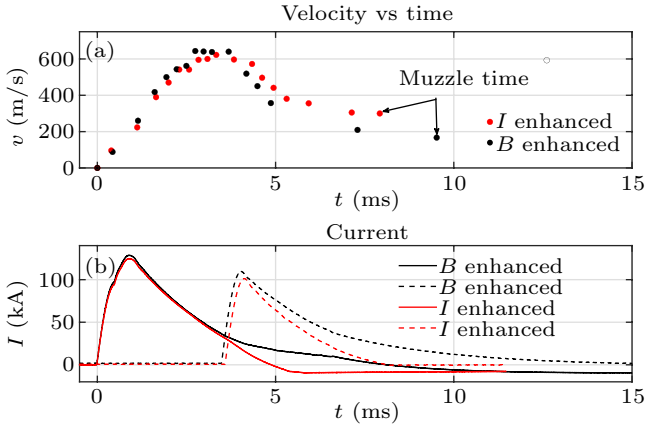


Fig. 12. (a) Comparation of armature velocity under current enhanced connection mode (red dot) and magnetic enhanced connection mode (black dot). (b) The experimental current flow of the current enhanced acceleration (red line) and deceleration (red dash line) processes, together with the experimental current flow of the magnetic enhanced acceleration (black line) and deceleration (black dash line) processes.

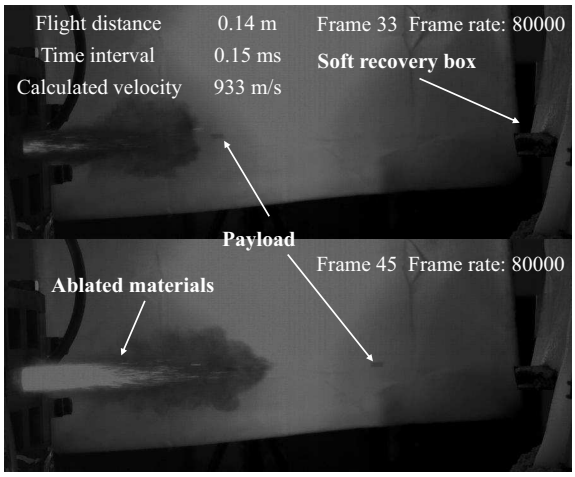


Fig. 13. Separated payload flying out of the muzzle.

To test the separation of the payload from the armature, a dummy pellet made of carbon was inserted into the guide block which was attached to the armature, as shown in Fig. 5. The mass of the pellet was 100 mg according to the DMS requirement for J-TEXT. The separation tests were carried out successfully and the maximum muzzle velocity of the payload exceeded 900 m/s while the minimum muzzle velocity was 294 m/s. Figure 13 shows the payload flying out of the muzzle ahead of other impurities and the decelerated armature. Most of the separation tests were carried out successfully except a

few pellets which were fractured before flying out of the muzzle because of the excessive assembling stress. Further optimization and test would be carried out to realize a precise control of the pellet speed and assure the separation of the entire pellet.

The experimental results show that EMPI has the ability to launch pellet at high speed in a short reaction time. And the armature can be recovered in a short distance. However, transition and muzzle arc still exist in the prototype tests. Plasma arc will not only affect the launch efficiency, but also enhance the rail ablation, reduce the lifetime of the rails, and produce a certain amount of metal impurities. To deal with this problem, X-type armature[16] was designed. In the experiment, X-type armature showed a high deceleration efficiency and maintained a good contact state in the deceleration process, which effectively suppressed the transition. In addition to the modifications of the armature, the use of tungsten, chromium and other ablative metal coating on the surface of the rail will also be conducive to the suppression of the arc in bore. Meanwhile, an enhanced rail configuration will be designed and tested on the EMPI-2. With a lower armature current, the ablation of the rails and armature would be greatly weakened, thus suppressing the arc in bore. For muzzle arc, a combined active–passive arc suppression system is also being designed and tested. It is expected that the implementation of the above scheme will greatly reduce the impact of arc on launch and make EMPI feasible to be used in disruption mitigation of tokamak.

5. Conclusion and perspectives

An EMPI configuration has been proposed as a massive material injector for DMS to realize fast response, high velocity and high reliable pellet injection for disruption mitigation. The prototype shows good performance in pellet launching, armature decelerating and pellet releasing. A maximum armature velocity of 1210 m/s has been achieved during the bench test. An overall response time of less than 10 ms could be achieved for J-TEXT with a minimum velocity of 572 m/s. Pellet in-bore release test has also been carried out successfully and a maximum pellet velocity of 900 m/s has been achieved while the armature is decelerated to less than 200 m/s. The trajectory of the pellet after separation is also traced along the injection axis.

The test results are encouraging, and the EMPI configuration has been primarily verified. However, some improvements are needed before being applied to tokamak devices. Despite the use of solid armature as propeller, rail erosion still remains. A certain amount of impurity would be generated when the condition of the contact surface grows worse. To deal with the problems and carry on the test in vacuum environment, design and construction of EMPI-2 are on the schedule. It is expected that with the improvement, EMPI-2 would be able to be equipped on the J-TEXT tokamak and perform disruption mitigation experiments.

Acknowledgments

The authors are very grateful for the help of the J-TEXT team. Project supported by the National Magnetic Confinement Fusion Energy Research and Development Program of China (Grant No. 2019YFE03010004) and the National Natural Science Foundation of China (Grant Nos. 12175078, 11905077, and 51821005).

References

[1] Lehnen M, Aleynikova K, Aleynikov P B, Campbell D J, Drewelow P, Eidietis N W, Gasparyan Y, Granetz R S, Gribov Y, Hartmann N, Hollmann E M, Izzo V A, Jachmich S, Kim S H, Kočan M, Koslowski H R, Kovalenko D, Kruezi U, Loarte A, Maruyama S, Matthews G F, Parks P B, Pautasso G, Pitts R A, Reux C, Riccardo V, Roccella R, Snipes J A, Thornton A J and de Vries P C 2015 *J. Nucl. Mater.* **463** 39

[2] Lehnen M, Jachmich S and Kruezi U 2020 *IAEA Technical Meeting on Plasma Disruptions and their Mitigation*, July 20–23, 2020, Vienna, Austria

[3] Hollmann E M, Aleynikov P B, Fülöp T, Humphreys D A, Izzo V A, Lehnen M, Lukash V E, Papp G, Pautasso G, Saint-Laurent F and Snipes J A 2015 *Phys. Plasmas* **22** 021802

[4] Lehnen M, Alonso A, Arnoux G, Baumgarten N, Bozhenkov S A, Brezinsek S, Brix M, Eich T, Gerasimov S N, Huber A, Jachmich S, Kruezi U, Morgan P D, Plyusnin V V, Reux C, Riccardo V, Sergienko G and Stamp M F 2011 *Nucl. Fusion* **51** 123010

[5] Bakhtiari M, Kawano Y, Tamai H, Miura Y, Yoshino R and Nishida Y 2002 *Nucl. Fusion* **42** 1197

[6] Lukash V E, Mineev A B and Morozov D K 2007 *Nucl. Fusion* **47** 1476

[7] Commaux N, Baylor L R, Jernigan T C, Hollmann E M, Parks P B, Humphreys D A, Wesley J C and Yu J H 2010 *Nucl. Fusion* **50** 112001

[8] Herfindal J L, Shiraki D, Baylor L R, Eidietis N W, Hollmann E M, Lasnier C J and Moyer R A 2019 *Nucl. Fusion* **59** 106034

[9] Vega J, Dormido-Canto S, López J M, Murari A, Ramírez J M, Moreno R, Ruiz M, Alves D and Felton R 2013 *Fusion Eng. Des.* **88** 1228

[10] Hawke R S 1983 *J. Vac. Sci. Technol. A* **1** 969

[11] Combs S K, Meitner S J, Baylor L R, Caughman J, Commaux N, Fehling D T, Foust C R, Jernigan T C, McGill J M, Parks P B and Rasmussen D A 2010 *IEEE Trans. Plasma Sci.* **38** 400

[12] Chen C, Lan T, Xiao C, Zhuang G, Kong D, Zhang S B, Zhang S, Ding W, Wu Z, Mao W, Wu J, Xu H, Wu J, Zu Y, Zhang D, Wei Z, Wen X, Zhou C, Liu A, Xie J, Li H and Liu W 2022 *Plasma Sci. Technol.* **24** 045102

[13] Raman R, Lay W S, Jarboe T, Menard J and Ono M 2018 *Nucl. Fusion* **59** 016021

[14] Raman R, Lunsford R, Clauser C F, Jardin S C, Menard J E and Ono M 2021 *Nucl. Fusion* **61** 126034

[15] Raman R, Jarboe T R, Menard J E, Gerhardt S P, Ono M, Baylor L and Lay W S 2015 *Fusion Sci. Technol.* **68** 797

[16] Zhongyong C, Weikang Z, Junhui T, Feng L and Shengguo X 2022 *Trans. China Electrotech. Soc.* **037** 5056